



# A continuum model for the mechanical behavior of nanowires including surface and surface-induced initial stresses

F. Song<sup>a</sup>, G.L. Huang<sup>a,b,\*</sup>, H.S. Park<sup>c</sup>, X.N. Liu<sup>b</sup>

<sup>a</sup> Department of Applied Science, University of Arkansas at Little Rock, Little Rock, AR 72204, USA

<sup>b</sup> Department of Systems Engineering, University of Arkansas at Little Rock, Little Rock, AR 72204, USA

<sup>c</sup> Department of Mechanical Engineering, Boston University, Boston, MA 02215, USA

## ARTICLE INFO

### Article history:

Received 5 August 2010

Received in revised form 18 March 2011

Available online 25 March 2011

### Keywords:

Surface stress

Surface initial stress

Continuum modeling

Nanowires

## ABSTRACT

The continuum modeling of the mechanical behavior of nanowires has recently attracted much attention due to its simplicity and efficiency. However, there are still some critical issues to be solved. In this paper, we demonstrate the importance of accounting for the effects of initial stresses in the nanowires that are caused by deformation due to surface stresses; we note that such initial stresses have previously been neglected in most existing continuum models. By considering the local geometrical nonlinearity of strains during the incremental flexural motion, a new formulation of the Euler–Bernoulli beam model for nanowires is developed through the incremental deformation theory, in which effects of the surface stress, the surface-induced initial stress and surface elasticity are naturally incorporated. It is found through comparisons to existing experimental and computational results for both fcc metal and ceramic nanowires that the surface-induced initial stresses, which are neglected in the Young–Laplace model, can significantly influence the overall mechanical properties of nanowires. We additionally demonstrate and quantify the errors induced by using the Young–Laplace model due to its approximation of surface stresses acting on only the top and bottom surfaces of nanowires.

© 2011 Elsevier Ltd. All rights reserved.

## 1. Introduction

Nanowires (NWs) have been intensely investigated due to their potential as the basic building blocks for nanoelectromechanical systems (Craighead, 2000; Feng et al., 2007). The significant surface effects on the mechanical behavior of NWs with increasing surface-to-volume ratio have been observed both theoretically and experimentally (Sharma et al., 2003; Mcdowell et al., 2008; Philippe et al., 2009). Various numerical approaches have also been developed to capture the distinct size dependence of NWs due to surface stresses including the molecular simulation (MS) (Park and Ji, 2006; Karpov et al., 2006; Agrawal et al., 2008; Zhang and Huang, 2009; Jiang and Batra, 2009; Park et al., 2009; Wang et al., 2010a) and various finite element-based approaches that account for surface effects in different ways (Park et al., 2006; Wei et al., 2006; Park and Klein, 2007; Yvonnet et al., 2008; Park and Klein, 2008; Yun and Park, 2009; He and Lilley, 2009; She and Wang, 2009; Javili and Steinmann, 2010).

For the sake of simplicity and efficiency, analytical continuum approaches are also highly attractive (Gurtin and Murdoch, 1978;

Zhang et al., 2004; He et al., 2004; Lu et al., 2006; Huang, 2008; Bar On et al., 2010), and thus the bending and buckling behavior of NWs has been studied by using the classical beam theory integrated with (Gurtin and Murdoch's) linear surface elasticity theory (He and Lilley, 2008a,b; Wang and Feng, 2009). In these models, surface effects on the flexural deformation are considered by using the generalized Young–Laplace equation (Chen et al., 2006a), which results in an equivalent distributed loading term in the beam equation. However, there are still some open problems with respect to the success of such formulation. First, the Young–Laplace model (He and Lilley, 2008a,b) cannot correctly predict the bending behavior of NWs with different boundary conditions. For fixed/fixed NWs, good agreement between the model and experiments (Cuenot et al., 2004; Jing et al., 2006) is found for Pb and Ag NWs, respectively, where both predict a significant size-dependent stiffening of the Young's modulus (He and Lilley, 2008a). In contrast, significant discrepancy is observed for fixed/free NWs; specifically, the experiment by Zijlstra et al. (2008) found that the elastic moduli of free standing [100] Au nanorods agree well with the bulk values, but size variation of the effective Young's modulus is reflected by the Young–Laplace model (He and Lilley, 2008b). The Young–Laplace model also incorrectly predicts the recently experimentally observed size-dependent Young's modulus of silicon nitride nanocantilevers (Gavan et al., 2009). Specifically,

\* Corresponding author at: Department of Systems Engineering, University of Arkansas at Little Rock, Little Rock, AR 72204, USA. Tel.: +1 5016837522; fax: +1 5015698698.

E-mail address: [glhuang@ualr.edu](mailto:glhuang@ualr.edu) (G.L. Huang).

the Young–Laplace model predicts elastic softening based on the first resonant frequency, but elastic stiffening if based upon the second resonant frequency (Gavan et al., 2009).

One key reason for these errors resulting from the Young–Laplace model is because the effects of the surface-induced initial stresses are neglected in the Young–Laplace model (He and Lilley, 2008a,b). These effects can be critical due to the large deformations, including phase transformations and axial reorientations, that surface stresses are known to cause in NWs, which have been both predicted computationally and observed experimentally (Park and Klein, 2007; Yun and Park, 2009; Diao et al., 2003; Park et al., 2005; Liang et al., 2005a; Huang et al., 2008; Desai and Haque, 2007; Tao et al., 2007; Agrawal et al., 2008; Richter et al., 2009). Furthermore, these internal initial stresses and large elastic deformations induced by surface stresses can influence the overall mechanical properties (Liang et al., 2005b), such as the stiffness and the resonant frequency, and therefore the dynamic behavior of NWs. Zhang et al. (2008) proposed a continuum model that considers the residual strain to study the surface stress effects on Young’s modulus and yield strength of NWs. The effects of surface stresses and initial stresses on the yield strength of NWs were studied (Zhang et al., 2008). However, for the beam or nanobeam structures, Gurtin et al. (1976) and Lu et al. (2005) showed that the residual surface stresses have no effect on the resonant frequency if linear elastic kinematics are considered. To date, there has been no study that has considered the effects of the surface-induced initial stresses upon the flexural behavior of NWs by using nonlinear strain measurements.

In the present paper, we begin with an analysis of the surface-induced initial stresses in the bulk and surface of NWs based on the Gurtin and Murdoch’s surface elasticity theory (Gurtin and Murdoch, 1975). After derivation of the surface-induced initial stresses in NWs, a new formulation of the Euler–Bernoulli beam model is developed through the incremental deformation theory by considering the local geometrical nonlinearity of the Lagrangian strain components during the incremental flexural motion (Biot, 1965; Sun, 1972; Song and Huang, 2009). Therefore, the effects of surface stresses, surface-induced initial stresses and surface elasticity are naturally incorporated into the modified Euler–Bernoulli beam equation. From our newly derived governing equation, we additionally demonstrate that the surface stresses along the cross sectional perimeter of the NW have contributions not only on the loading term but also on the effective bending rigidity of the NWs in the equation of motion during the incremental deformation. The comparison of the current model and the Young–Laplace model for NWs with different boundary conditions is also discussed.

Results from the current model are compared with those from the existing experimental measurements, the surface Cauchy–Born (SCB) model (Park and Klein, 2008) and the Young–Laplace model (He and Lilley, 2008a,b; Wang and Feng, 2009). Very good agreement among the current model, experimental data and the SCB model shows the validity of the current model and the importance of including the surface-induced initial stresses in the continuum model of NWs. Both fixed/free and fixed/fixed boundary conditions for the bending deformation of NWs are discussed and compared; we further compare our results for both metallic and ceramic NWs. As compared to existing experimental data and numerical results, the current model which accounts for both the effects of the surface stresses and surface-induced initial stresses provides a very reasonable prediction of dynamic bending behavior for both the fixed/fixed and fixed/free NWs. However, the Young–Laplace model cannot correctly reflect the resonant frequency shift, as demonstrated by examples with fixed/free NWs, and also in considering surface effects on the higher mode resonant frequencies of NWs.

## 2. Continuum model

### 2.1. Determination of surface-induced initial stresses

Even in the absence of external loading, both modeling and experiments have shown that surface stresses can cause significant deformation of NWs (Liang et al., 2005b; Huang et al., 2008; Zhang et al., 2008; Yun and Park, 2009; Jiang and Batra, 2009), where the amount of deformation depends upon the boundary conditions. We first consider an undeformed NW without any surface stresses, referred to as the original state. A linear elastic surface with the initial surface stress  $\tau_0$  is then attached to the NW; due to this initial surface stress, the NW will undergo an initial deformation until an equilibrium state is reached which is referred to as the relaxed state, as shown in Fig. 1. In the study, for the fixed/free boundary condition, the NW will initially undergo axial relaxation that is tensile or compressive depending on the material, which results in a redistribution of the surface and surface-induced initial stresses. For the fixed/fixed boundary condition, the surface stress in the original state of the NW is the same as that in the relaxed state of the NW, and no deformation will be initiated due to the constraints at the ends of the NW.

In this study, the mathematical ‘surface’ with zero thickness is assumed based on the surface elasticity theory (Gurtin and Murdoch, 1975). Determination of the relaxed state of the NWs can be achieved by the potential energy minimization (Zhang et al., 2008). The surface-induced initial axial stress and strain are assumed to be constant within the cross sections of the NWs in the study. Therefore, the axial initial stress  $\tilde{\sigma}_{xx}$  and strain  $\tilde{\epsilon}_{xx}$  within the NW are given by

$$\tilde{\sigma}_{xx} = E\tilde{\epsilon}_{xx} \quad (1)$$

in which  $E$  is the bulk Young’s modulus of the NW, and the embellishment “ $\tilde{\bullet}$ ” represents the relaxed state. The surface stresses can be expressed by the surface elasticity theory as

$$\tilde{\tau}_{xx} = \tau_0 + E_s\tilde{\epsilon}_{xx}^s, \quad (2)$$

where  $\tilde{\tau}_{xx}$  is the total initial surface stress,  $E_s$  is the surface modulus, and  $\tilde{\epsilon}_{xx}^s$  is the initial surface strain in the relaxed state. The continuity condition between the bulk and surface requires  $\tilde{\epsilon}_{xx}^s = \tilde{\epsilon}_{xx}$  at the surface. In the absence of any external loading, the system potential energy can be written as

$$\Pi = U_V + U_S = \left( \int_0^{\tilde{\epsilon}_{xx}} \tilde{\sigma}_{xx} d\tilde{\epsilon}_{xx} \right) A + \left( \int_0^{\tilde{\epsilon}_{xx}^s} \tilde{\tau}_{xx} d\tilde{\epsilon}_{xx}^s \right) C, \quad (3)$$

where  $U_V$  and  $U_S$  denote deformation energies within the NW and its surface, respectively,  $A$  is the area and  $C$  the perimeter of NW cross section. The minimization of  $\Pi$  determines the  $\tilde{\epsilon}_{xx}^s$  (or  $\tilde{\epsilon}_{xx}$ ) and hence  $\tilde{\tau}_{xx}$  and  $\tilde{\sigma}_{xx}$  for the relaxed state, which should be considered as the initial state for the bending analysis hereafter. For fixed/fixed NWs, we have  $\tilde{\epsilon}_{xx}^s = \tilde{\epsilon}_{xx} = 0$  because the constraints at the ends of the NW prevent the axial relaxation. In summary, before the bending deformation, the following initial (relaxed) state due to surface stresses should be considered in the NW for different boundary conditions

$$\tilde{\sigma}_{xx} = \begin{cases} -\frac{EC}{EA+E_sC} \tau_0, & \text{fixed/free NWs,} \\ 0, & \text{fixed/fixed NWs,} \end{cases} \quad (4)$$

$$\tilde{\tau}_{xx} = \begin{cases} \frac{EA}{EA+E_sC} \tau_0, & \text{fixed/free NWs,} \\ \tau_0, & \text{fixed/fixed NWs.} \end{cases} \quad (5)$$

It should be mentioned that the relaxed configuration of the NWs depends not only on the boundary conditions but also on the specific fabrication processes. In this study, the following assumptions

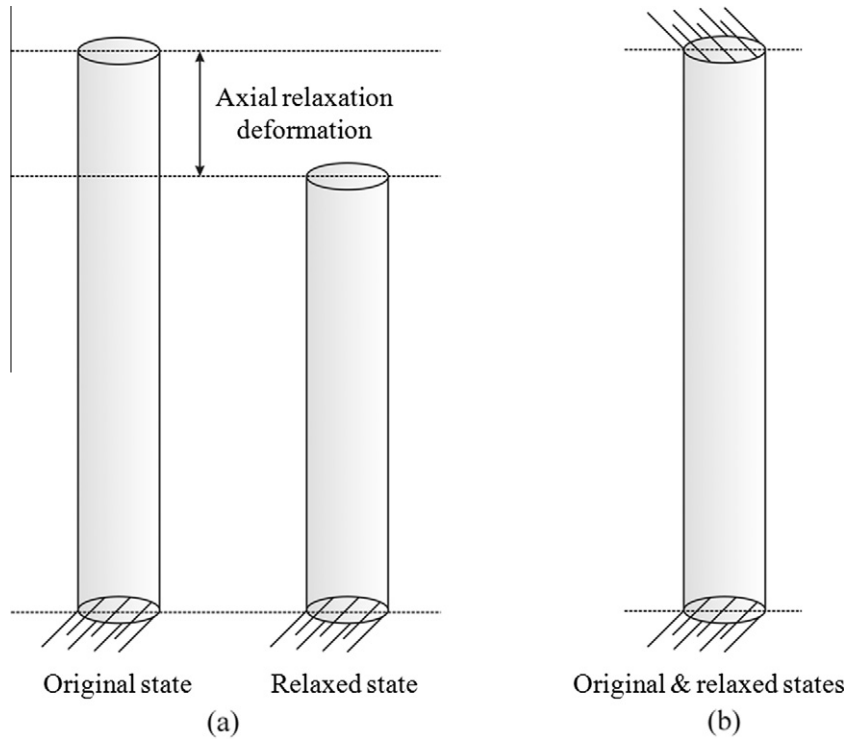


**Fig. 1.** Illustrations of boundary effects on configurations of NWs at different states with: (a) fixed/free; (b) fixed/fixed boundary conditions; note that the axial deformation for the fixed/free boundary condition can either be compressive (for fcc metals), or tensile (for silicon).

are made for NWs with different boundary conditions in Eqs. (4) and (5):

- (i) For the fixed/free boundary condition, the derivation of surface and surface-induced initial stresses is based on the NWs with free relaxation configuration. This assumption is good for NWs that are fabricated via bottom-up growth processes, such as the chemical vapor deposition method (Gavan et al., 2009), the thermal evaporation approach (Chen et al., 2006b), the vapor–liquid–solid growth (Wu and Yang, 2001) and the seed mediated growth techniques (Nikoobkht and El-Sayed, 2003; Zijlstra et al., 2008).
- (ii) For the fixed/fixed boundary condition, the derivation of surface and surface-induced initial stresses is based on the NWs with constrained relaxation configuration. This assumption is good for NWs that are created via etching or top-down fabrication processes, for which the NWs are being constrained before the etching. This assumption is also consistent with many prior computational studies of NWs (Park and Klein, 2008; Yun and Park, 2009; Makeev et al., 2006; Wang et al., 2010b).
- (iii) The relaxation along the transverse directions of the NW due to surface stresses is neglected in the current model.

## 2.2. Beam theory with surface and surface-induced initial stresses

We now consider the bending deformation of a straight NW in the  $x$ – $z$  plane, as shown in Fig. 2. According to the Euler–Bernoulli beam assumption, the displacement field in the NW can be expressed as

$$u_x(x, z, t) = -z \frac{\partial w(x, t)}{\partial x}, \quad u_z(x, z, t) = w(x, t), \quad (6)$$

where  $z$  denotes the coordinate measured from the NW's neutral plane. The nonlinear Green–Lagrangian strain of the NW can be expressed by

$$e_{xx} = -z \frac{\partial^2 w}{\partial x^2} + \frac{1}{2} \left( z \frac{\partial^2 w}{\partial x^2} \right)^2 + \frac{1}{2} \left( \frac{\partial w}{\partial x} \right)^2. \quad (7)$$

According to the theory of Trefftz (Biot, 1965; Sun, 1972), the total bulk and surface stresses can be assumed to be related linearly to the accompanying strain as

$$\sigma_{xx}^t = \tilde{\sigma}_{xx} + E e_{xx}, \quad (8)$$

$$\tau_{xx}^t = \tilde{\tau}_{xx} + E_s e_{xx}^s, \quad (9)$$

where the superscript  $s$  denotes the surface quantity.

The linear incremental constitutive relation is adopted here, because the incremental deformation from the relaxed state is assumed to be infinitesimal. However, the strain–displacement relations must be nonlinear because the effects of the axial initial bulk and surface stresses on the transverse deflection depend on the existence of the geometrical nonlinearity of the Lagrangian strain components, as shown in Eq. (7). With the linear stress–strain relations using Eqs. (8) and (9), the strain energy of the NW per unit initial volume is readily obtained as

$$W_b = \int_0^{e_{xx}} \sigma_{xx}^t d e_{xx} = \left( \tilde{\sigma}_{xx} + \frac{1}{2} E e_{xx} \right) e_{xx} \quad (10)$$

for the bulk, and

$$W_s = \int_0^{e_{xx}^s} \tau_{xx}^t d e_{xx}^s = \left( \tilde{\tau}_{xx} + \frac{1}{2} E_s e_{xx}^s \right) e_{xx}^s \quad (11)$$

for the surface where  $e_{xx}^s = e_{xx}$  at the surface.

According to the theory of Biot (1965), the incremental potential energy of the NW is pertinent in the variational formulation:

$$\Delta W = \Delta W_b + \Delta W_s, \quad (12)$$

where  $\Delta W_b = W_b - \tilde{\sigma}_{xx} e_{xx}$  and  $\Delta W_s = W_s - \tilde{\tau}_{xx} e_{xx}^s$  with  $e_{xx} = \partial u_x / \partial x$  being the usual linear strain, and  $e_{xx}^s = e_{xx}$  at the surface.

Substituting Eqs. (10) and (11) into Eq. (12), the total incremental potential energy per unit initial length of the NW can be ob-

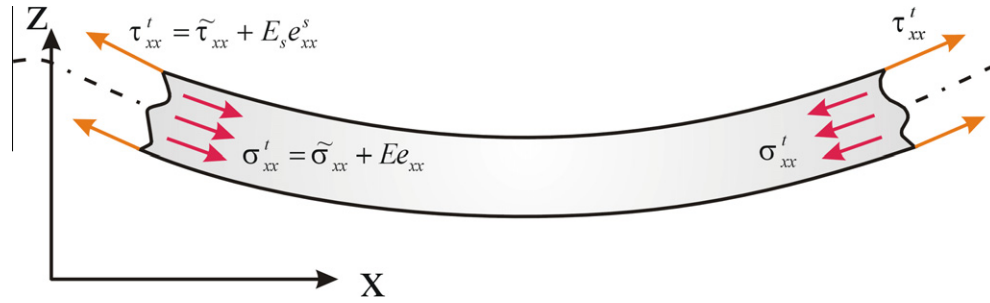


Fig. 2. Schematic of the relevant bulk and surface stresses during the bending deformation of a NW.

tained by integrating  $\Delta W$  over the cross section and surface, respectively, as

$$U = \frac{1}{2} \left[ (\tilde{\sigma}_{xx} I + \tilde{\tau}_{xx} I_s + E_s I_s + EI) \left( \frac{\partial^2 w}{\partial x^2} \right)^2 + (\tilde{\sigma}_{xx} A + \tilde{\tau}_{xx} C) \left( \frac{\partial w}{\partial x} \right)^2 \right], \quad (13)$$

where  $I$  is the moment of inertia, and  $I_s$  is the surface moment of inertia. The kinetic energy per unit length of the NW is expressed as

$$T = \frac{1}{2} \rho A \left( \frac{\partial w}{\partial t} \right)^2. \quad (14)$$

By applying Hamilton's principle based on Eqs. (13) and (14), the flexural equation of motion of the NWs including the combined effects of the surface stresses and surface-induced initial stresses is obtained as

$$\rho A \frac{\partial^2 w}{\partial t^2} + (EI)^* \frac{\partial^4 w}{\partial x^4} - P^* \frac{\partial^2 w}{\partial x^2} = 0, \quad (15)$$

where for circular NWs,  $P^* = \pi a^2 \tilde{\sigma}_{xx} + 2\pi a \tilde{\tau}_{xx}$ ,  $(EI)^* = EI + \tilde{\sigma}_{xx} I + (E_s + \tilde{\tau}_{xx}) I_s$ ,  $I = \pi a^4 / 4$ ,  $I_s = \pi a^3$  and  $a$  is the radius. For rectangular NWs,  $P^* = bh \tilde{\sigma}_{xx} + 2(b+h) \tilde{\tau}_{xx}$ ,  $(EI)^* = EI + \tilde{\sigma}_{xx} I + (E_s + \tilde{\tau}_{xx}) I_s$ ,  $I = bh^3 / 12$ ,  $I_s = bh^2 / 2 + h^3 / 6$  and  $b$  and  $h$  are the width and thickness, respectively.

As shown in Eq. (15), the initial surface stresses  $\tilde{\sigma}_{xx}$  and  $\tilde{\tau}_{xx}$ , as defined in Eqs. (1) and (2), contribute to both the loading term  $P^*$  and effective bending rigidity  $(EI)^*$ ; this is because we have considered the local geometrical nonlinearity of the Lagrangian strain components. Therefore, the overall mechanical behavior of the NWs will be affected by the initial surface stresses. Simulation results from the current model will be compared with those from the existing experimental measurements, the SCB model and the generalized Young–Laplace model to show the importance of considering the surface-induced initial stresses.

### 2.3. Comparison with Young–Laplace model

It is also interesting to note that the governing Eq. (15) derived by the current model has the same form as that of the Young–Laplace model (He and Lilley, 2008b) except for the detailed formulation of the loading term and the effective bending rigidity. We now discuss fundamental differences between the current model and the Young–Laplace model, where for consistency of comparison, the surface-induced initial stress is ignored in the current model. Based on this assumption, the loading term and the effective bending rigidity in Eq. (15) can be reduced for NWs with circular (Cir) and rectangular (Rec) cross sections, respectively, as listed in Table 1. For comparison, the loading term  $P^*$  and effective bending rigidity  $(EI)^*$  in the Young–Laplace model (He and Lilley, 2008a,b; Wang and Feng, 2009) are also included in Table 1.

Table 1

Comparison of the current model without the surface-induced initial stresses with the Young–Laplace model (He and Lilley, 2008a,b; Wang and Feng, 2009).

	Loading term $P^*$	Effective bending rigidity $(EI)^*$
The current model without initial stresses	Cir: $2\pi a \tau_0$	Cir: $EI + (E_s + \tau_0) \pi a^3$
	Rec: $2(b+h)\tau_0$	Rec: $EI + (E_s + \tau_0)(bh^2/2 + h^3/6)$
The Young–Laplace model	Cir: $4a\tau_0$	Cir: $EI + E_s \pi a^3$
	Rec: $2b\tau_0$	Rec: $EI + E_s(bh^2/2 + h^3/6)$

The difference of the effective bending rigidities  $(EI)^*$  between the two models originates from the fact that the effects of the surface stress are included in the current model by considering the local geometrical nonlinearity, which is ignored in the Young–Laplace model. In addition, according to the Young–Laplace model, only surface stresses on the top and bottom surfaces of NWs can enter the loading term in the governing equation for NWs with rectangular cross section, and surface stresses on the side surfaces are absent (He and Lilley, 2008a,b). This formulation therefore neglects the important contribution of surface stresses acting on the side surfaces, which impacts the system energy during the bending deformation, and hence the governing equation. This is clearly unphysical as any preexisting stress, regardless of whether it occurs in the bulk or the surface, should be accounted for if they contribute to the strain energy. The generalized Young–Laplace model was originally derived to address interface/surface tension between two different solids incorporating the interface stresses (Chen et al., 2006a). The model is based on the classical theory of membranes under in-plane surface stresses. Therefore, the Young–Laplace model can correctly capture the effects of surface stresses on the top and bottom surfaces with nonzero curvatures during bending deformation (Gurtin and Murdoch, 1975; Gurtin et al., 1976; Wang and Feng, 2007). However, if the Young–Laplace model is adopted for NWs (e.g. He and Lilley, 2008a,b), the effects of surface stresses on the side surfaces cannot be captured because the side surfaces have zero bending curvatures. From the comparison of the derivation in Table 1, it can be found that the Young–Laplace model may be a good approximation only for micro/nanobeams with a large width-to-thickness ratio of the cross section, but it may not be applicable for NWs where the cross section has comparable width and thickness dimensions. The comparison of the current model and the Young–Laplace continuum model for NWs with different boundary conditions are now discussed via numerical examples and existing experimental data.

### 3. Numerical results

To validate the current model, experimental measurements for the effective Young's modulus of silicon nitride (SiNx) nanocantile-



vers (Gavan et al., 2009) will be first compared with those obtained using the current model and the Young–Laplace model. It was reported in the experimental paper that the Young–Laplace model gives a contradictory result for the effective Young’s modulus based on the measured first and second mode resonant frequencies, respectively (Gavan et al., 2009). Specifically, size-dependent elastic softening is predicted by the Young–Laplace model based upon the first resonant frequency, while size-dependent elastic stiffening is predicted based upon the second resonant frequency.

Fig. 3 shows the effective Young’s modulus predictions of the SiNx fixed/free nanocantilever with respect to different thicknesses based on the current model, the Young–Laplace model (He and Lilley, 2008b) and existing experimental measurements (Gavan et al., 2009) by using the first and second resonant frequencies, respectively. In the figure, the effective Young’s modulus is calculated as  $E_{eff} = (f^*)^2 E$  with  $f^*$  being the ratio of the resonant frequency calculated with the surface and surface-induced initial stresses to that calculated without the surface and surface-induced initial stresses (Weaver et al., 1990). The fixed dimensions of the cantilever are the length ( $L = 60 \mu\text{m}$ ) and the width ( $b = 12 \mu\text{m}$ ). The bulk material properties of the cantilever are Young’s modulus ( $E = 300 \text{ GPa}$ ) and mass density ( $\rho = 3100 \text{ kgm}^{-3}$ ) (Gavan et al., 2009). There are no published values of surface elastic properties for amorphous SiNx; therefore, we utilize the surface properties of the cantilever given in Gavan et al. (2009), i.e.  $\tau_0 = 0.1 \text{ N/m}$  and  $E_s = -1070 \text{ N/m}$ . From the figure, it can be found that the Young–Laplace model (He and Lilley, 2008b) gives inconsistent predictions about the effective Young’s modulus of the cantilever that is predicted by using the first and the second resonant frequencies, respectively. To explain the discrepancy, an ad hoc surface elasticity model was suggested by Gavan et al. (2009), in which the residual surface stress term  $\tau_0$  in the Young–Laplace equation was ignored.

In contrast, as shown in Fig. 3, the current model predictions are consistent with the experimental results by using both the first and second resonant frequencies, in which the surface-induced initial stress is considered. The explanation based on the current model is that for the fixed/free boundary condition the loading term  $P^*$  in Eq. (15), which represents the combined effects of the surface initial stress and the bulk initial stress, vanishes based on their relationship in Eqs. (4) and (5). Therefore, the first and second res-

onant frequencies are only related to the effective bending rigidity  $(EI)^*$  for the fixed/free nanocantilever, in which the effects of the initial stress are included in the current model. Therefore, the effective Young’s modulus is predicted consistently by using the first and second frequencies.

However, for the Young–Laplace model, the first and second resonant frequencies are influenced by both the non-vanishing loading term and the effective Young’s modulus. Neglect of the surface-induced initial stress results in the non-vanishing loading term, as listed in Table 1. The non-vanishing loading term (the transverse force) is the reason for the inconsistent prediction about the effective Young’s modulus of the cantilever in the Young–Laplace model. For the first mode, the signs of the non-vanishing transverse force and displacement are the same which causes softening of the effective Young’s modulus. However, for the second mode, the signs of the non-vanishing transverse force and displacement are opposite which causes stiffening of the effective Young’s modulus. A detailed physical explanation for the contradictory result can also be found in Gavan et al. (2009).

Both numerical simulation and experimental testing have been widely utilized to characterize the size-dependent elastic moduli of NWs and nanorods (Mcdowell et al., 2008; Park and Klein, 2008; Agrawal et al., 2008; Cuenot et al., 2004; Jing et al., 2006; Chen et al., 2006b; Zijlstra et al., 2008). In the following, the comparison of the current model, the Young–Laplace model (He and Lilley, 2008a,b), the SCB model (Park and Klein, 2008) and the experimental measurement (Chen et al., 2006b; Zijlstra et al., 2008) for predictions of effective Young’s modulus of NWs and nanorods with different boundary conditions is discussed.

While many experimental tests of NWs with fixed/free boundary conditions have been reported (Cuenot et al., 2004; Jing et al., 2006; Mcdowell et al., 2008), there have been comparably fewer published experimental results of NWs with fixed/free boundary conditions. Fig. 4 shows the comparison of the effective Young’s modulus of fixed/free ZnO NWs with an axial [0001] orientation with  $(10\bar{1}0)$  surfaces as a function of the diameter by the current model, the Young–Laplace model (He and Lilley, 2008b) and the existing experimental measurement (Chen et al., 2006b). To our best knowledge, there are no rigorous values published for both bulk and surface properties of ZnO NWs in a single paper. In the

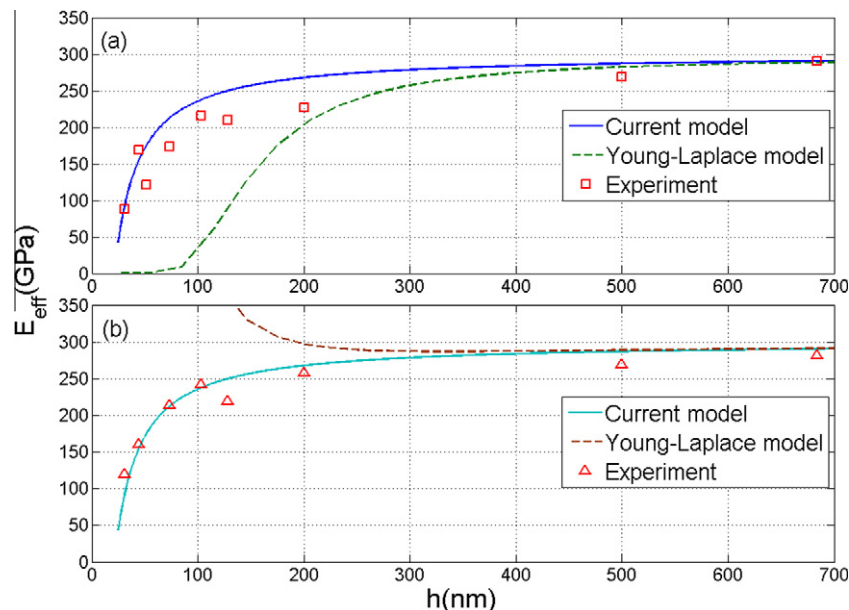


Fig. 3. The effective Young’s modulus prediction of the SiNx cantilever based on the current model, the Young–Laplace model (He and Lilley, 2008b) and experimental testing data (Gavan et al., 2009): (a) the first mode and (b) the second mode.

calculation, the bulk Young’s modulus in [0001] oriented ZnO NWs is selected as  $E = 140$  GPa from (Chen et al., 2006b), and the density  $\rho = 5.6 \times 10^3 \text{ kgm}^{-3}$  from (Pauporte et al., 2002); the surface stress is used as  $\tau_0 = -0.91 \text{ N/m}$  for (10 $\bar{1}0$ ) surface of ZnO from the first-principles method (Wang and Li, 2007), and the surface modulus for [0001] oriented ZnO NWs is used as  $E_s = 267 \text{ N/m}$  in Xu et al. (2010), which was obtained by data fitting with experimental measurements. The experimental specimens in Chen et al. (2006b) have typical lengths of 7–15  $\mu\text{m}$  and no variation of the Young’s modulus with the slight increase in length was observed (Chen et al., 2006b); therefore, the length of the ZnO NWs is assumed as  $L = 10 \mu\text{m}$  for the calculations in this work. The effective Young’s modulus is obtained as  $E_{eff} = (f^*)^2 E$  where  $f^*$  is defined as the ratio of the resonant frequency calculated with the surface and surface-induced initial stresses to that calculated without the surface and surface-induced initial stresses.

For the fixed/free ZnO NWs, the current model gives an excellent prediction of the effective Young’s modulus of the NWs with different diameters compared with those in the experimental measurements. However, the Young–Laplace model overestimates the effective Young’s modulus of the NWs, especially for the NWs with small diameters because the surface stress effects on the fixed/free NWs are overestimated by the Young–Laplace model. The physical explanation is that for the NWs with the fixed/free boundary condition, the free end of the NWs undergoes relaxation due to surface stresses, and therefore the surface-induced initial stresses should be considered. However, for the Young–Laplace model, the initial stress is always ignored, thus leading to an artificially stiff elastic response.

As previously discussed, the axial surface relaxation of the NW is different for brittle ceramic materials (e.g., ZnO) as compared to fcc metals (e.g., Ag and Au). To show the capability of the current

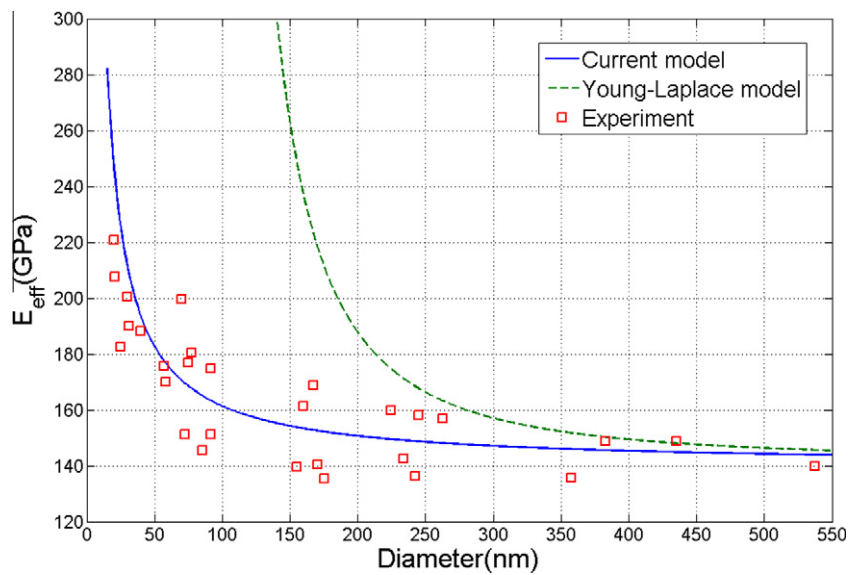


Fig. 4. Comparison of the effective Young’s modulus  $E_{eff}$  of fixed/free ZnO NWs as a function of the diameter obtained from the current model, the Young–Laplace model (He and Lilley, 2008b), and the existing experimental measurement (Chen et al., 2006b).

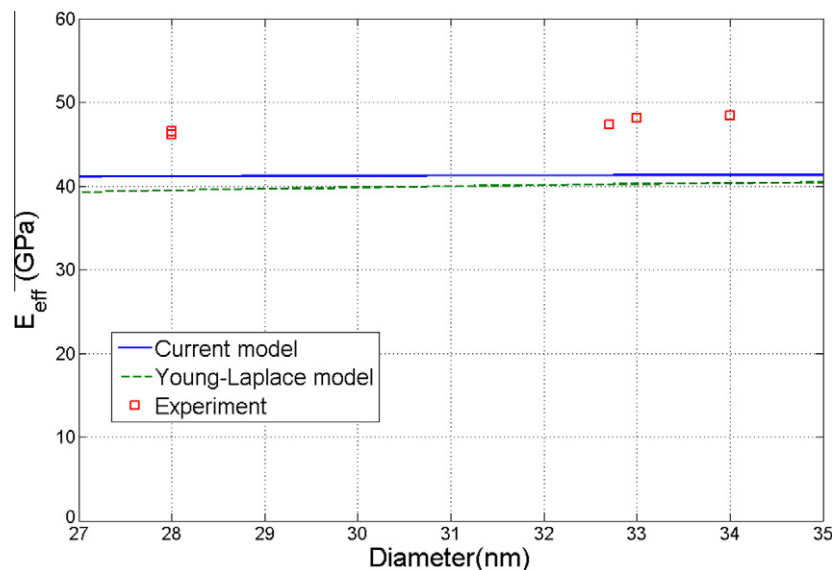


Fig. 5. Comparison of the effective Young’s modulus  $E_{eff}$  of free standing Au Nanorods as a function of diameters obtained from the current model, the Young–Laplace model (He and Lilley, 2008b), and existing experimental data (Zijlstra et al., 2008).

model, the effective Young's modulus  $E_{eff}$  of fixed/free Au nanorods predicted by the current model, the Young–Laplace model (He and Lilley, 2008b) and existing experimental data (Zijlstra et al., 2008) is illustrated and compared in Fig. 5. In the figure, the effective Young's modulus is calculated as  $E_{eff} = (f^*)^2 E$  where  $f^*$  is defined as the ratio of the resonant frequency with the surface and surface-induced initial stresses to that without the surface and surface-induced initial stresses. The experimental effective Young's modulus is based on measurements of the extensional mode frequency (Zijlstra et al., 2008). The nanorods are [100] Au and the average length  $L = 92$  nm is used in the calculation. The bulk material properties of the nanorods are the Young's modulus ( $E = 42$  GPa) (Zijlstra et al., 2008) and mass density ( $\rho = 19.3 \times 10^3$  kgm<sup>-3</sup>), and the surface properties of [100] Au crystal with (100) surface are  $\tau_0 = 1.4$  N/m and  $E_s = -3.6$  N/m (Shenoy, 2005). From the figure, it can be found that the current model shows al-

most no size dependence of the effective Young's modulus for fixed/free Au nanorods, which is consistent with the experimental observation by Zijlstra et al. (2008). However, small variation of the effective Young's modulus with respect to size can be observed by using the Young–Laplace model (He and Lilley, 2008b), even when the nanorods have small aspect ratios which significantly reduce the surface stress effects. The stiffening of the measured modulus over the bulk value was attributed to coupling to the substrate (Zijlstra et al., 2008) or possible impurity of the single crystal structure of the nanorod, which is not reflected in the current model and the Young–Laplace model (He and Lilley, 2008b).

We now investigate the mechanical behavior of metal (Au) NWs using the resonant frequencies computed by different models to show the importance of considering the surface-induced initial stress for different boundary conditions. Fig. 6 shows the comparison of the fundamental resonant frequency shift of the NW pre-

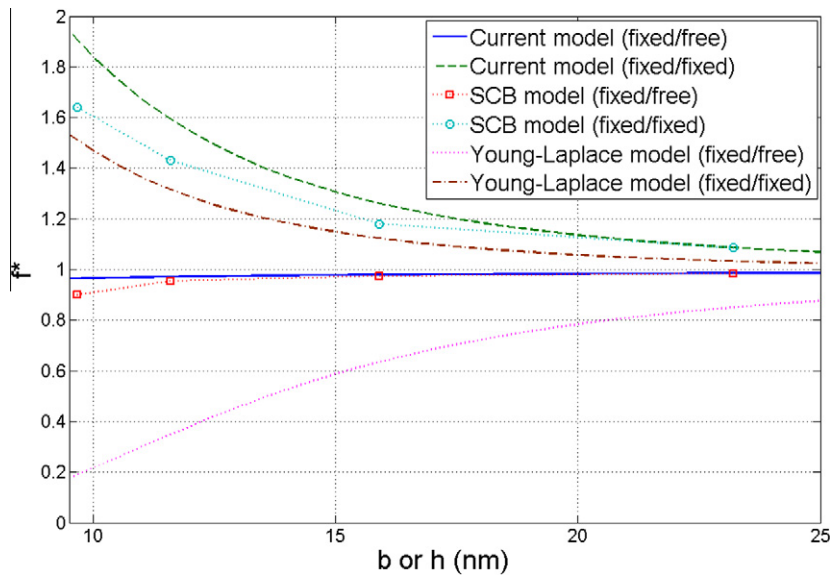


Fig. 6. The comparison of the fundamental resonant frequency shift of the constant length square Au NWs as a function of NW width ( $b$ ) or thickness ( $h$ ) from the current model, the Young–Laplace model (He and Lilley, 2008b) and the SCB model (Park and Klein, 2008).

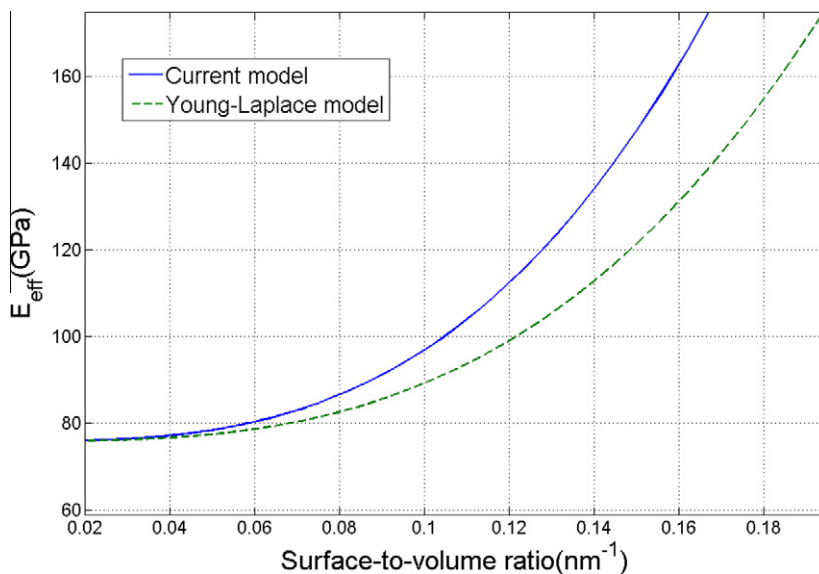
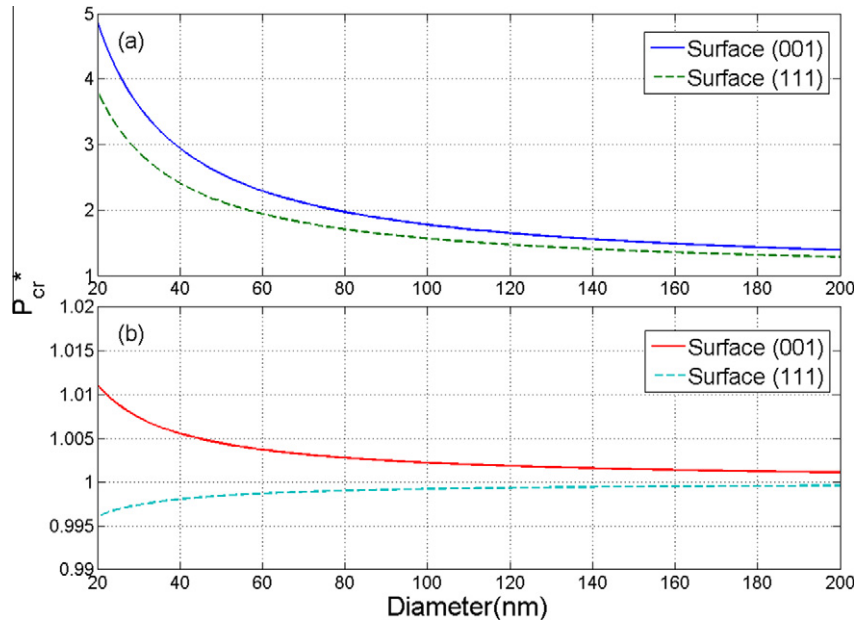


Fig. 7. Comparison of the effective Young's modulus  $E_{eff}$  of fixed/fixed Ag NWs as a function of surface-to-volume ratio obtained from the current model and the Young–Laplace model (He and Lilley, 2008a).



**Fig. 8.** The critical compressive load of axial buckling of circular Ag NWs with different surface orientations as a function of the NW diameter. (a) The Young–Laplace model (Wang and Feng, 2009) and (b) the current model.

dicted by the current model, the SCB model (Park and Klein, 2008) and the Young–Laplace model (He and Lilley, 2008b) respectively. Both the fixed/fixed and fixed/free NWs are considered. The NW is square [100] Au of the constant length ( $L = 232$  nm) (Park and Klein, 2008). The bulk material properties of the NW are Young's modulus ( $E = 35$  GPa) and mass density ( $\rho = 19.3 \times 10^3$  kgm $^{-3}$ ) (Park and Klein, 2008), and the surface properties of the NW are  $\tau_0 = 1.4$  N/m and  $E_s = -3.6$  N/m (Shenoy, 2005). In the figure, the normalized resonant frequency  $f^*$  is defined as the ratio of the resonant frequency calculated with the surface and surface-induced initial stresses to that calculated without the surface and surface-induced initial stresses.

First, as expected, the frequency shift results from both the current model and the Young–Laplace model agree reasonably well with that by the SCB model for the fixed/fixed NWs, because the surface-induced initial stresses disappear due to the constraints at two ends of the NW and this physical situation is identical for all the models. However, compared with the Young–Laplace model, the current model can provide a better prediction and finally converges to the SCB model with an increase in the NW cross sectional dimension. For the fixed/free NW, the current model still agrees very well quantitatively with the SCB model. However, significant discrepancy between the current model and the Young–Laplace model can be observed which occurs because the Young–Laplace model dramatically overestimates the surface stress effects by ignoring the effects of the initial stress.

To further quantify the discrepancies between the current model and Young–Laplace model, Fig. 7 shows the comparison of the effective Young's modulus of the fixed/fixed circular Ag NW with varying surface-to-volume ratio predicted by the current model and the Young–Laplace model (He and Lilley, 2008a). The effective Young's modulus  $E_{eff}$  is obtained based on the bending deflection equivalency by the conventional Euler beam model without the surface stresses (He and Lilley, 2008a). The properties of the (001) surface of Ag are  $\tau_0 = 0.89$  N/m and  $E_s = 1.22$  N/m (Shenoy, 2005), while the bulk Young's modulus of Ag is taken as  $E = 76$  GPa (Jing et al., 2006). The fixed length of the NW is  $L = 1$   $\mu$ m (He and Lilley, 2008a). To our best knowledge, there are no corresponding experimental measurements available for the

fixed/fixed NWs fabricated in a top-down manner. From Fig. 7, it can be observed that both the current model and the Young–Laplace model can predict the general stiffening tendency of the effective Young's modulus of the Ag NWs with increasing surface-to-volume ratio. This is primarily because for the fixed/fixed boundary condition in the current model, the surface-induced initial stresses vanish because the constraints at the ends of the NW prevent the axial relaxation; this physical situation is identical to what is represented for this boundary condition by the Young–Laplace model. Therefore, similar results are obtained for both models without the initial stress. However, the Young–Laplace model quantitatively underestimates the effective Young's modulus of the NW with small cross sectional dimensions, which occurs because the Young–Laplace model does not take into account the effects of the surface stresses on the lateral side surfaces. The detailed difference between the current model and Young–Laplace model can be found in Table 1 for the fixed/fixed NWs.

For our final numerical example in illustrating the difference in predictions obtained using the current model and the Young–Laplace model, we investigate the effects of surface stresses on the buckling behavior of fixed/free NWs under uniaxial compression. The critical axial force of buckling is derived as  $P_{cr} = \pi^2(EI)^* / (4L^2) + P^*$  for the fixed/free NW (Wang and Feng, 2009). For the Ag NWs,  $E = 76$  GPa;  $\tau_0 = 0.89$  N/m and  $E_s = 1.22$  N/m are used for the (001) surface, and  $\tau_0 = 0.65$  N/m and  $E_s = -1.39$  N/m for the (111) surface orientation (Shenoy, 2005). Fig. 8 demonstrates the critical compressive buckling loads of the NW with respect to the diameter predicted by the Young–Laplace model (Wang and Feng, 2009) and the current model, respectively. In the figure, the normalized buckling load  $P_{cr}^*$  is defined as the ratio of the critical axial force with the surface and surface-induced initial stresses to that without the surface and surface-induced initial stresses. As shown in the figure for the current model, the critical compressive force of buckling becomes greater with the presence of surface stress for the Ag NWs with (001) surfaces, while it becomes smaller for (111) surfaces. However, for the Young–Laplace model, the critical compressive force of buckling increases with the decrease of the diameter of Ag NWs with both (001) and (111) surfaces (Wang and Feng, 2009). It is interesting to point out that the surface



effects on the buckling loads of the NW predicted by the current model are much smaller than the predictions using the Young–Laplace model as shown in Fig. 8. This is expected because the surface stress effects on the effective Young's modulus of the fixed/free NW are overestimated without considering the surface initial stress by using Young–Laplace model, and also for the buckling behavior of the NW. We also note that recent experimental results on silicon NWs also indicated that the critical buckling force of the NW shows little deviation from that expected from classical linear elastic theory (Hsin et al., 2008).

#### 4. Conclusion

In summary, we have demonstrated the importance of accounting for surface-induced initial stresses, which are neglected in most existing continuum models, on both the bulk and the surfaces of nanowires. By considering the geometrically nonlinear strains, a new formulation of the Euler–Bernoulli beam model of nanowires is developed through the incremental deformation theory, in which effects of the surface stress, the surface-induced initial stress and surface elasticity are naturally incorporated. We demonstrate through comparisons to existing experimental and computational results the fact that surface-induced initial stresses, which are neglected in the commonly used Young–Laplace model, have a significant effect on the size and boundary condition-dependent mechanical properties of metallic and ceramic nanowires. Furthermore, we demonstrated that the Young–Laplace model is also in error due to the fact that it considers the effects of surface stresses on only the top and bottom surfaces of the nanowires.

#### Acknowledgements

GLH acknowledges funding from the NSF-EPS-0701890. HSP acknowledges funding from the NSF-CMMI 0750395. The authors would also like to thank one of the anonymous reviewers for his/her pertinent comments and invaluable suggestions.

#### References

- Agrawal, R., Peng, B., Gdoutos, E., Espinosa, H.D., 2008. Elasticity size effects in ZnO nanowires—A combined experimental–computational approach. *Nano Lett.* 8, 3668–3674.
- Bar On, B., Altus, E., Tadmor, E.B., 2010. Surface effects in non-uniform nanobeams: continuum vs atomistic modeling. *Int. J. Solids Struct.* 47, 1243–1252.
- Biot, M.A., 1965. *Mechanics of Incremental Deformations*. Wiley, New York.
- Chen, T., Chiu, M.S., Weng, C.N., 2006a. Derivation of the generalized Young–Laplace equation of curved interfaces in nanoscaled solids. *J. Appl. Phys.* 100, 074308.
- Chen, C.Q., Shi, Y., Zhang, Y.S., Zhu, J., Yan, Y.J., 2006b. Size dependence of Young's modulus in ZnO nanowires. *Phys. Rev. Lett.* 96, 075505.
- Craighead, H.G., 2000. Nanoelectromechanical systems. *Science* 290, 1532–1535.
- Cuenot, S., Fretigny, C., Demoustier-Champagne, S., Nysten, B., 2004. Surface tension effect on the mechanical properties of nanomaterials measured by atomic force microscopy. *Phys. Rev. B* 69, 165410.
- Desai, A.V., Haque, M.A., 2007. Mechanical properties of ZnO nanowires. *Sensors Actuat. A Phys.* 134, 169–176.
- Diao, J., Gall, K., Dunn, M.L., 2003. Surface-stress-induced phase transformation in metal nanowires. *Nature Mater.* 2, 656–660.
- Feng, X.L., He, R.R., Yang, P.D., Roukes, M.L., 2007. Very high frequency silicon nanowire electromechanical resonators. *Nano Lett.* 7, 1953–1959.
- Gavan, K.B., Westra, H.J.R., Venstra, W.J., van der Drift, E.W.J.M., van der Zant, H.S.J., 2009. Size-dependent effective Young's modulus of silicon nitride cantilevers. *Appl. Phys. Lett.* 94, 233108.
- Gurtin, M.E., Murdoch, A.I., 1975. A continuum theory of elastic material surfaces. *Arch. Rat. Mech. Anal.* 57, 291–323.
- Gurtin, M.E., Markenscoff, X., Thurston, R.N., 1976. Effect of surface stress on the natural frequency of thin crystals. *Appl. Phys. Lett.* 29, 529.
- Gurtin, M.E., Murdoch, A.I., 1978. Surface stress in solids. *Int. J. Solids Struct.* 14, 431–440.
- He, L.H., Lim, C.W., Wu, B.S., 2004. A continuum model for size-dependent deformation of elastic films of nano-scale thickness. *Int. J. Solids Struct.* 41, 847–857.
- He, J., Lilley, C.M., 2008a. Surface effect on the elastic behavior of static bending nanowires. *Nano Lett.* 8, 1798–1802.
- He, J., Lilley, C.M., 2008b. Surface stress effect on bending resonance of nanowires with different boundary conditions. *Appl. Phys. Lett.* 93, 263108.
- He, J., Lilley, C.M., 2009. The finite element absolute nodal coordinate formulation incorporated with surface stress effect to model elastic bending nanowires in large deformation. *Comput. Mech.* 44, 395–403.
- Huang, D.W., 2008. Size-dependant response of ultra-thin films with surface effects. *Int. J. Solids Struct.* 45, 568–579.
- Huang, W.J., Sun, R., Tao, J., Menard, L.D., Nuzzo, R.G., Zuo, J.M., 2008. Coordination-dependent surface atomic contraction in nanocrystals revealed by coherent diffraction. *Nature Mater.* 7, 308–313.
- Hsin, C.-L., Mai, W., Gu, D., Gao, Y., Huang, C.-T., Liu, Y., Chen, L.-J., Wang, Z.-L., 2008. Elastic properties and buckling of silicon nanowires. *Adv. Mater.* 20, 3919–3923.
- Javili, A., Steinmann, P., 2010. A finite element framework for continua with boundary energies Part II: the three dimensional case. *Comput. Meth. Appl. Mech. Eng.* 199, 755–765.
- Jiang, W., Batra, R.C., 2009. Molecular statics simulations of buckling and yielding of gold nanowires deformed in axial compression. *Acta Mater.* 57, 4921–4932.
- Jing, G.Y., Duan, H.L., Sun, X.M., Zhang, Z.S., Xu, J., Li, Y.D., Wang, J.X., Yu, D.P., 2006. Surface effects on elastic properties of silver nanowires: contact atomic-force microscopy. *Phys. Rev. B* 73, 235409.
- Karpov, E.G., Yu, H., Park, H.S., Wang, J.Q., Liu, W.K., Qian, D., 2006. Multiscale boundary conditions in crystalline solids: theory and application to nanoindentation. *Int. J. Solids Struct.* 43, 6359–6379.
- Liang, W., Zhou, M., Ke, F., 2005a. Shape memory effect in Cu nanowires. *Nano Lett.* 5, 2039–2943.
- Liang, H.Y., Upmanyu, M., Huang, H.C., 2005b. Size-dependent elasticity of nanowires: nonlinear effects. *Phys. Rev. B* 71, 241403.
- Lu, P., He, L.H., Lee, H.P., Lu, C., 2006. Thin plate theory including surface effects. *Int. J. Solids Struct.* 43, 4631–4647.
- Lu, P., Lee, H.P., Lu, C., O'Shea, S.J., 2005. Surface stress effects on the resonance properties of cantilever sensors. *Phys. Rev. B* 72, 085405.
- Makeev, M.A., Srivastava, D., Menon, M., 2006. Silicon carbide nanowires under external loads: an atomistic simulation study. *Phys. Rev. B* 74, 165303.
- Mcdowell, M.T., Leach, A.M., Gall, K., 2008. On the elastic modulus of metallic nanowires. *Nano Lett.* 8, 3613–3618.
- Nikoobkht, B., El-Sayed, M.A., 2003. Preparation and growth mechanism of gold nanorods (NRs) using seed-mediated growth method. *Chem. Mater.* 15, 1957–1962.
- Park, H.S., Gall, K., Zimmerman, J.A., 2005. Shape memory and pseudoelasticity in metal nanowires. *Phys. Rev. Lett.* 95, 255504.
- Park, H.S., Ji, C., 2006. On the thermomechanical deformation of silver shape memory nanowires. *Acta Mater.* 54, 2645–2654.
- Park, H.S., Klein, P.A., Wagner, G.J., 2006. A surface Cauchy–Born model for nanoscale materials. *Int. J. Numer. Meth. Eng.* 68, 1072–1095.
- Park, H.S., Klein, P.A., 2007. Surface Cauchy–Born analysis of surface stress effects on metallic nanowires. *Phys. Rev. B* 75, 085408.
- Park, H.S., Klein, P.A., 2008. Surface stress effects on the resonant properties of metal nanowires: the importance of finite deformation kinematics and the impact of the residual surface stress. *J. Mech. Phys. Solids* 56, 3144–3166.
- Park, H.S., Cai, W., Espinosa, H.D., Huang, H., 2009. Mechanics of crystalline nanowires. *MRS Bull.* 34, 178–183.
- Pauporte, Th., Cortes, R., Froment, M., Beaumont, B., Lincot, D., 2002. Electrocrystallization of epitaxial zinc oxide onto gallium nitride. *Chem. Mater.* 14, 4702–4708.
- Philippe, L., Wang, Z., Peyrot, I., Hassel, A.W., Michler, J., 2009. Nanomechanics of rhenium wires: elastic modulus, yield strength and strain hardening. *Acta Mater.* 57, 4032–4035.
- Richter, G., Hillerich, K., Gianola, D.S., Monig, R., Kcraft, O., Volkert, C.A., 2009. Ultrahigh strength single crystalline nanowhiskers grown by physical vapor deposition. *Nano Lett.* 9, 3048–3052.
- Sharma, P., Ganti, S., Bhat, N., 2003. Effect of surfaces on the size-dependent elastic state of nano-inhomogeneities. *Appl. Phys. Lett.* 82, 535–537.
- She, H., Wang, B., 2009. A geometrically nonlinear finite element model of nanomaterials with consideration of surface effects. *Finite Element Anal. Des.* 45, 463–467.
- Shenoy, V.B., 2005. Atomistic calculations of elastic properties of metallic fcc crystal surfaces. *Phys. Rev. B* 71, 094104.
- Song, F., Huang, G.L., 2009. Modeling of surface stress effects on bending behavior of nanowires: incremental deformation theory. *Phys. Lett. A* 373, 3969–3973.
- Sun, C.T., 1972. On the equations for a Timoshenko beam under initial stress. *J. Appl. Mech. (Trans. ASME)* 39, 282–285.
- Tao, X., Wang, X., Li, X., 2007. Nanomechanical characterization of one-step combustion-synthesized Al<sub>4</sub>B<sub>2</sub>O<sub>9</sub> and Al<sub>18</sub>B<sub>4</sub>O<sub>33</sub> nanowires. *Nano Lett.* 7, 3172–3176.
- Wang, G., Li, X., 2007. Size dependency of the elastic modulus of ZnO nanowires: surface stress effect. *Appl. Phys. Lett.* 91, 231912.
- Wang, G.F., Feng, X.Q., 2007. Effects of surface elasticity and residual surface tension on the natural frequency of microbeams. *Appl. Phys. Lett.* 90, 231904.
- Wang, G.F., Feng, X.Q., 2009. Surface effects on buckling of nanowires under uniaxial compression. *Appl. Phys. Lett.* 94, 141913.
- Wang, Z.G., Li, J.B., Gao, F., Weber, W.J., 2010a. Tensile and compressive mechanical behavior of twinned silicon carbide nanowires. *Acta Mater.* 58, 1963–1971.
- Wang, Z.-J., Liu, C., Li, Z., Zhang, T.-Y., 2010b. Size-dependant elastic properties of Au nanowires under bending and tension-surface versus core nonlinearity. *J. Appl. Phys.* 108, 083506.

- Weaver, W., Timoshenko, S.P., Young, D.H., 1990. *Vibration Problems in Engineering*. Wiley, New York.
- Wei, G., Shouwen, Y., Ganyun, H., 2006. Finite element characterization of the size-dependent mechanical behaviour in nanosystems. *Nanotechnology* 17, 1118–1122.
- Wu, Y., Yang, P., 2001. Direct observation of vapor–liquid–solid nanowire growth. *J. Am. Chem. Soc.* 123, 3165–3166.
- Xu, F., Qin, Q., Mishra, A., Gu, Y., Zhu, Y., 2010. Mechanical properties of ZnO nanowires under different loading modes. *Nano Res.* 3, 271–280.
- Yun, G., Park, H.S., 2009. Surface stress effects on the bending properties of fcc metal nanowires. *Phys. Rev. B* 79, 195421.
- Yvonnet, J., Quang, H.L., He, Q.-C., 2008. An XFEM/level set approach to modelling surface/interface effects and to computing the size-dependent effective properties of nanocomposites. *Comput. Mech.* 42, 119–131.
- Zhang, W.X., Wang, T.J., Chen, X., 2008. Effect of surface stress on the asymmetric yield strength of nanowires. *J. Appl. Phys.* 103, 123527.
- Zhang, Y., Huang, H., 2009. Do twin boundaries always strengthen metal nanowires? *Nanoscale Res. Lett.* 4, 34–38.
- Zhang, Y., Ren, Q., Zhao, Y.P., 2004. Modelling analysis of surface stress on a rectangular cantilever beam. *J. Phys. D Appl. Phys.* 37, 2140–2145.
- Zijlstra, P., Tchebotareva, A.L., Chon, J.W.M., Gu, M., Orrit, M., 2008. Acoustic oscillations and elastic moduli of single gold nanorods. *Nano Lett.* 8, 3493–3497.